

Cite this: *Nanoscale*, 2018, **10**, 12109

Tumor-targeted and nitric oxide-generated nanogels of keratin and hyaluronan for enhanced cancer therapy†

Zhe Sun, Zeng Yi, Xinxing Cui, Xiangyu Chen, Wen Su, Xiaoxiang Ren and Xudong Li *

The development of safe and effective nano-drug delivery systems to deliver anticancer drugs to targeted cells and organs is crucial to enhance the therapeutic efficacy and overcome unwanted side effects of chemotherapy. Herein, we prepared CD44-targeted dual-stimuli responsive human hair keratin and hyaluronic acid nanogels (KHA-NGs) through a simple crosslinking method. KHA-NGs, which consisted of spheres 50 nm in diameter, were used as carriers to load the anticancer drug doxorubicin hydrochloride (DOX). The drug release, cellular uptake, cytotoxicity, and targeting ability of DOX-loaded KHA-NGs (DOX@KHA-NGs) were assessed *in vitro* and the anticancer effects were further evaluated *in vivo*. The DOX@KHA-NGs had a super-high drug loading capacity (54.1%, w/w) and were stable under physiological conditions (10 µM glutathione (GSH)), with the drug being rapidly released under a tumor cell microenvironment of trypsin and 10 mM GSH. Cellular uptake and *in vitro* cytotoxicity results indicated that DOX@KHA-NGs specifically targeted cancer cells and effectively inhibited their growth. Furthermore, KHA-NGs were capable of improving intracellular nitric oxide levels, which sensitizes the cells and enhances the anticancer efficacy of chemotherapeutic drugs. *In vivo* experiments showed that DOX@KHA-NGs had a better anti-tumor effect and lower side effects compared to free DOX. These results suggest that the bio-responsive KHA-NGs have potential applications for targeted cancer therapy.

Received 20th April 2018,

Accepted 11th June 2018

DOI: 10.1039/c8nr03265c

rsc.li/nanoscale

1. Introduction

In order to increase the curative effect and reduce the unwanted side effects of chemotherapeutic drugs, novel drug carriers such as liposomes, porous nanoparticles, and surface-coated drug nanoparticles have been developed.^{1–4} However, despite their remarkable advantages,^{5–9} the effectiveness of these carriers is limited by the non-specific targeting^{10,11} and lack of controlled drug release.^{12,13} Moreover, an insufficient drug loading capacity further decreases their therapeutic efficacy and their non-specific accumulation in visceral organs leads to serious unwanted side effects, thus limiting their clinical applications.^{14,15}

Human hair keratin is an abundant, renewable resource with outstanding biological functions, including biocompat-

ability, bioactivity, and no immunogenicity.¹⁶ The cysteine- and sulphydryl-rich structure of human hair keratin enables it to degrade by enzymes.^{17,18} Keratin has abundant side groups, including carboxyl, amino or sulphydryl groups, which allows its functionalization with various biomolecules to improve the stability, drug loading capacity, targeting ability, etc.^{18–21} Additionally, the keratin chain can degrade into small segments, such as non-toxic peptides and amino acids, which are easily metabolized *in vivo*.²² Moreover, keratin can promote the production of intracellular nitric oxide (NO),^{23,24} which sensitizes tumor cells, thus enhancing the anticancer efficacy of chemotherapeutic drugs.²⁵

Based on the enhanced permeability and retention (EPR) effect,^{26,27} recent studies have focused on the preparation of drug carriers with tumor-specific active targeting agents that can conjugate specific ligands of tumor cells in order to enhance the accumulation effect at the tumor site.^{28–33} Hyaluronic acid (HA) is a natural polysaccharide that can bind to cell-specific surface markers such as cluster determinant 44 (CD44) receptors, which are over-expressed on the cytomembrane of several different tumor cells, including melanoma, breast and lymphoma tumor cells.^{34,35} The linear structure of HA comprises alternating units of D-glucuronic acid and

National Engineering Research Center for Biomaterials, Sichuan University, Chengdu 610064, People's Republic of China. E-mail: xli20004@yahoo.com; Fax: +86 (0)288541 2102; Tel: +86 (0)28 8541 2102

† Electronic supplementary information (ESI) available: Detailed methods contain cell culture, animal tumor model, histological examination and immunohistochemical analysis and *ex vivo* imaging studies. See DOI: 10.1039/c8nr03265c

N-acetyl-d-glucosamine, linked by β -1,3- and β -1,4-glycosidic bonds. The negative charge and good hydrophilicity of HA promote the absorption of multiple layers of drug molecules onto its surface.³⁶ Additionally, HA has excellent biodegradability, biocompatibility, and non-immunogenicity,^{37–39} which afford it with great potential applications as an anticancer drug carrier.

Herein, we prepared keratin-hyaluronic acid nanogels (KHA-NGs) as targeted drug carriers with stimuli response and high doxorubicin hydrochloride (DOX) loading efficacy to achieve an anti-cancer therapeutic effect both *in vitro* and *in vivo*. KHA-NGs were synthesized through a hydrogen bonding and oxidation reaction under mild conditions, leading to the formation of spheres of 50 nm in diameter (Scheme 1). The crosslinked structure with abundant hydrophilic groups and negative charge allowed a high DOX loading efficiency (54.1%) to form DOX-loaded KHA-NGs (DOX@KHA-NGs). The release of loaded DOX was triggered by a change in pH or trypsin or GSH concentration in the intracellular environment. Compared to free DOX, DOX@KHA-NGs showed CD44 ligand binding function and a better inhibition effect on cancer cells *in vitro*, likely due to the increment in NO levels stimulated by keratin. The therapeutic effect and toxicity of DOX@KHA-NGs were further investigated *in vivo*. The present study shows that the KHA-NGs are promising nano-drug carriers for targeting tumor therapy.

2. Experimental

2.1 Materials

Human hair was donated from several healthy Chinese females (24–27 years old, no dyeing or perming). HA ($\geq 95\%$, 10 kDa), ethanol, urea, thiourea, 2-mercaptoethanol, sodium dodecyl sulfate (SDS) and Tris-HCl were purchased from KL Biochem Ltd (Chengdu, China). Roswell Park Memorial

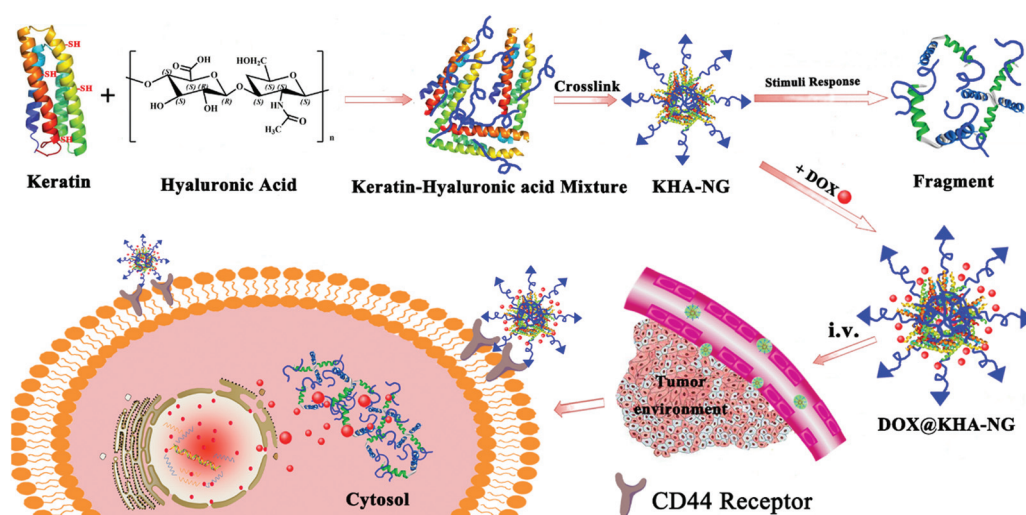
Institute (RPMI)-1640 cell culture medium, fetal calf serum, and penicillin-streptomycin antibiotics were obtained from Gibco (USA). Deionized water ($18 \text{ M}\Omega \text{ cm}^{-1}$) was used in all experiments. Doxorubicin hydrochloride (DOX, 99%) was purchased from Dalian Meilun bio Pharmaceuticals (China) and H_2O_2 (30%) from Jinshan Co. (China). Cell counting kit-8 (CCK-8) and Hoechst 33342 were obtained from Dojindo Molecular Technologies (Japan). *S*-Nitrosoglutathione (GSNO), Griess reagent kit and fluorescence indicator (3-amino,4-aminomethyl-2',7'-difluorescein, diacetate, DAF-FM DA) were purchased from Beyotime Biotech. Ltd (Shanghai, China). GSH and trypsin were obtained from Biosharp (Chengdu, China). All reagents and solvents were of analytical grade.

2.2 Extraction and identification of human hair keratins

In this study, human hair keratin was extracted from hair fibers based on previously reported methods with some modifications.¹⁶ Specifically, human hair was cleaned with ethanol and degreased with a mixture of isopropanol/methanol (2 : 1, v/v) for 24 h. The degreased hair (10 g) was then placed in 500 mL, pH 8.5 digestive solution (25 mM Tris-HCl, 2.6 M thiourea, 5 M urea, 5 g SDS, and 5% 2-mercaptoethanol) at 50 °C for 72 h. After that, the undigested hair residue was discarded and the digestive solution was collected and centrifuged at 12 000 rpm for 20 min at room temperature. The obtained liquid supernatant sample was dialyzed against deionized water using a dialysis bag (MWCO 14 kDa) with the dialysate water being replaced with distilled water every 6 h. The resulting sample was keratin solution and stored at 4 °C for further experiment.

2.3 Synthesis of KHA-NGs and keratin nanoparticles (KNPs)

KHA-NGs were synthesized using a simple two-step approach. Briefly, 1.25 mL of Tris-HCl (1 M), 10 g of thiourea, and 15 g of urea were added into a keratin solution (100 mL, 1 mg mL⁻¹) and stirred until dissolved. HA (30 mg) was then added into



Scheme 1 Schematic illustration of keratin-hyaluronic acid nanogels (KHA-NGs) and DOX@KHA-NGs for targeting cancer treatment.

the solution and the mixture was stirred continuously for 2 h under nitrogen atmosphere at room temperature. The mixture was then dialyzed in a 14 kDa dialysis bag to remove all inorganic salts and promote the development of hydrogen bonds, leading to the formation of a keratin-HA solution (KHA). The KHA solution was dried, weighed, and the mass concentration calculated. It was then attenuated to 0.1 mg mL⁻¹ and 0.5 mL of 30% H₂O₂ were added into 10 mL of the KHA solution whilst stirring. Under continuous stirring, the mixtures were placed in a water bath at 37 °C for 4 h. The products were then dialyzed in a 300 kDa dialysis bag to remove H₂O₂, as well as unreacted keratin and HA. The prepared KHA-NGs were then dried, weighed, and the mass concentration calculated, and stored at 4 °C. The synthesis of KNPs was similar to that of KHA-NGs, barring the addition of HA.

2.4 Preparation of DOX@KHA-NGs and DOX@KNPs

KHA-NGs and KNPs (0.25 mg mL⁻¹) were mixed with a DOX solution (1 mg mL⁻¹, pH 7.2–7.4) and stirred for 10 h at 4 °C. The mixtures were then centrifuged and the sediments collected and lyophilized to obtain DOX loaded KHA-NGs (DOX@KHA-NGs) and DOX loaded KNPs (DOX@KNPs), which were stored at 4 °C until further use. The supernatant was characterized *via* UV-vis absorption spectra and drug loading and encapsulation efficiencies were calculated. The standard curve of DOX was determined by taking the absorbance values DOX concentration between 0 and 250 µg mL⁻¹, which fit the Lambert-Beer law:

$$\text{Abs} = 0.0049 \times (C) + 0.0135 \quad R = 0.9996$$

where Abs and C represent the absorbance and the concentration (µg mL⁻¹), respectively. The drug loading efficiency (DL) and embedding ratio (ER) were calculated using the following equations.

$$\text{DL (wt\%)} = (W_{\text{DOX,L}}/W_{\text{DOX@KHA-NGs}}) \times 100\%$$

$$\text{ER (wt\%)} = (W_{\text{DOX,L}}/W_{\text{DOX-feeding}}) \times 100\%$$

where, $W_{\text{DOX,L}}$, $W_{\text{DOX@KHA-NGs}}$ and $W_{\text{DOX-feeding}}$ are the weight of DOX in the nanogels, the total weight of DOX@KHA-NGs and the weight of feeding DOX, respectively.

2.5 Characterization

The size, polydispersion index (PDI), and zeta potential of KNPs, KHA-NGs, DOX@KNPs, and DOX@KHA-NGs were determined by dynamic light scattering (DLS; Malvern Zeta-Sizer, UK). The nanoparticles and nanogels were characterized by transmission electron microscopy (TEM; FEI Tecnai G220, USA). Circular dichroism (CD) spectra of keratin and KHA-NGs were obtained using a Dichroism Spectropolarimeter JASCO model J-815 (Japan). FT-IR spectroscopy analysis was performed on a PerkinElmer Spectrum One B System with KBr pellets. X-ray photoelectron spectroscopy (XPS) was performed with a Kratos XSAM800 X-ray photoelectron spectrometer. UV-vis spectra was detected by a PerSee UV1901 spectrometer.

2.6 Stimuli response and release profile of DOX@KHA-NGs

To investigate the stimuli sensitivities, DOX@KNPs and DOX@KHA-NGs were incubated in different biomimetic environments, namely pure PBS buffer solution at pH 7.4, at pH 7.4 PBS buffer solution with 10 µM GSH, 10 mM GSH or 0.04 mM trypsin, pure PBS solution at pH 5.5, pH 5.5 PBS buffer solution with 10 mM GSH + 0.04 mM trypsin at 37 °C for 4 h. The morphology and average diameters of the nanoparticles and nanogels were examined by high resolution TEM (HRTEM). *In vitro* DOX releasing assay was performed in the following referred PBS buffers (pure PBS solution at pH 7.4, PBS solution at pH 5.5, 10 µM GSH, 10 mM GSH, trypsin, at pH 7.4 PBS solution and 10 mM GSH + 0.04 mM trypsin at pH 5.5 in PBS solution). Dialysis bags (MWCO 10 000 Da) containing 1 mL of DOX@KNPs or DOX@KHA-NGs mixture were soaked in tubes which contained 40 mL of different buffers, along with continuous shake at 37 °C (three samples per group). At the preset points of time (0, 0.5, 1, 1.5, 2, 2.5, 3, 4, 5, 8, 12, 24 and 48 h), 1 mL dialysis fluid was collected and an equal amount of fresh buffer was placed back. The concentration of DOX was measured by a UV-vis spectrophotometry (Persee TU-1901, China) at an excitation wavelength of 480 nm.

2.7 The effect of CD44 receptor blocking on intracellular distribution and cytotoxicity

Mouse breast cancer (4T1) cells (high CD44 expression) were incubated for 2 h with free hyaluronan (20 and 200 µg mL⁻¹). After 2 times of rinse with PBS, the cells were then replaced into fresh culture medium. DOX@KHA-NGs were added to the cell culture medium (DOX-equivalent dose: 5 µg mL⁻¹). After 4 h of incubation, the cells were stained with FITC (12 µg mL⁻¹) and Hoechst 33342 (5 µg mL⁻¹) for 10 min. The cells were rinsed with PBS thrice and observed under confocal laser scanning microscopy (CLSM). The excitation wavelengths were 340 nm (Hoechst 33342, Blue), 488 nm (FITC, Green), and 485 nm (DOX, Red). The emission wavelengths were 460 nm (Hoechst 33342, Blue), 530 nm (FITC, Green), and 595 nm (DOX, Red).

2.8 *In vitro* cytotoxicity study

Cell viability was measured with a CCK-8 assay. 4T1 and mouse melanoma B16 cells were seeded in 96-well plates at a density of 1×10^4 cells per well and cultured at 37 °C in a 5% CO₂ humidified incubator for 24 h. When the suitable cell confluence was 80%–90%, the media was discarded and then 100 µL fresh culture media containing DOX, DOX@KNPs or DOX@KHA-NGs was added into corresponding wells, respectively. In addition, cells cultured without drug treatment were regarded as a negative control. After 48 h of incubation, the cell viability was detected with CCK-8 kit.⁴⁰

4T1 and B16 cells (1×10^4 cells per well) were grown in 96-well plates for 24 h with free hyaluronan (200 µg mL⁻¹). Cells were cultured with different doses (DOX-equivalent dose: 1.25, 2.5, 5, 10, 20 µg mL⁻¹ at 4T1 cells and 0.25, 0.5, 1, 2,

$4 \mu\text{g mL}^{-1}$ at B16 cells) of DOX@KHA-NGs for 48 h and tested as above. All experiments were performed in triplicate.

L929 cells and NIH 3T3 cells (1×10^4 cells per well) were seeded in 96-well plates and cultured for 24 h. The culture media was then replaced with 100 μL of fresh media containing different concentrations (20, 10, 5, 2.5, 1.25 and 0.6125 $\mu\text{g mL}^{-1}$) of KHA-NGs and tested as above. The absorbance was measured at 450 nm on a Varioskan Microplate reader (Thermo Fisher Scientific, USA). The cell viability of 4T1 and B16 cells were calculated according the formula: $(\text{OD}_{\text{Sample}} - \text{OD}_{\text{Background}})/(\text{OD}_{\text{Control}} - \text{OD}_{\text{Background}}) \times 100\%$. All experiments were performed in triplicate.

2.9 Apoptosis assay

4T1 cells were seeded in 6-well plates and cultured for 24 h. The cells were incubated with culture medium containing saline, DOX, DOX@KHA-NGs, and DOX@KHA-NGs pretreated with 200 $\mu\text{g mL}^{-1}$ hyaluronan (5 $\mu\text{g mL}^{-1}$ DOX) for 36 h. The cells were collected after rinsing for three times and centrifugation, then incubated for 15 min with the Annexin V-FITC/PI Apoptosis Detection Kit (Dojindo, Japan) at room temperature in dark place. 4T1 cells were measured on a flow cytometer and detected the fluorescence signals at 515 nm for FITC and 615 nm for propidium iodide (PI).

2.10 Intracellular uptake

The cellular uptake behavior of DOX@KHA-NGs was determined by flow cytometry. 4T1 cells were seeded in 6-well plates (1×10^5 cells per well) for 24 h, and then treated with DOX, DOX@KNPs, DOX@KHA-NGs, or DOX@KHA-NGs (DOX-equivalent dose: 5 $\mu\text{g mL}^{-1}$) pretreated with 200 μg HA for 4 h. The medium without drug was set as control. Followed by rinsing with PBS and harvesting with trypsin, the cells were collected by centrifugation (1500 rpm, 5 min) and them resuspended in 1 mL of PBS. The cells were determined with a flow cytometer by counting at least 1×10^4 amounts per sample.

2.11 Nitric oxide generation detection and *in vitro* NO release

DAF-FM DA (Beyotime, Shanghai, China) was used as a fluorescence indicator of intracellular NO. Briefly, 4T1 cells were seeded in 35 mm Petri dishes at a density of 4×10^5 per well and dishes were divided into four groups. When the cells grown in petri dishes reached 80% confluence, they were washed three times with PBS solution and 1 mL of colorless serum-free medium (Solarbio) were added into each dish. A total of 5 μL (10 $\mu\text{g mL}^{-1}$) of keratin, KNPs, or KHA-NGs were added into the different groups and 5 μL of PBS solution was added into the fourth group as a control. Then, 50 μM of DAF-FM DA were loaded into each group and the cells were incubated at 37 °C for 4 h. Cells were then rinsed three times and maintained in colorless serum-free medium throughout the experiments. Images were captured randomly by an Olympus inverted fluorescence microscope (CKX53, Olympus, Tokyo, Japan) with a FITC parameter (excitation 494 nm, emission 518 nm).

NO release behavior was detected using Griess reagent. Briefly, 5 mL of the mixtures containing GSNO (65 μM), GSH (100 μM), and EDTA (500 μM) were prepared prior to use. After 48 h reaction of the weighted KHA-NGs (1.5 mg) in a screw-cap bottle at 37 °C, 50 μL of the solution was retrieved and placed into a 96-well plate. To each well, both Griess reagent I (50 μL) and Griess reagent II (50 μL) were added, and the wells were then incubated at room temperature for 20 min to form an azo-dye. The absorbance of the dye was monitored at 540 nm with a microplate reader and the amount of NO was quantified with NaNO₂ as a standard. The capacity to release NO was expressed as the concentration of NO₂. The mixed GSNO/GSH/EDTA solution without keratin, KNPs, or KHA-NGs was also tested as a blank.

2.12 *In vivo* antitumor activity

All experiments with live animals were performed in compliance with the relevant laws and institutional guidelines of Sichuan University and were approved by the ethics committee of the Sichuan University. Four week old BALB/c female mice were injected subcutaneously in the right flank with 5×10^6 4T1 murine breast cancer cells suspended in 100 μL of HEPES buffer solution (pH 7.4). Once tumors reached a size of 100–300 mm³ (calculated by $V = L \times W^2/2 \times \pi/3$, where L and W represent the largest and smallest diameters, respectively), mice were injected through the lateral tail vein with 100 μL of saline, DOX (5 mg kg⁻¹), DOX@KNPs (5 mg kg⁻¹, DOX equivalent), or DOX@KHA-NGs (5 mg kg⁻¹, DOX equivalent) ($n = 5$ /treatment) every three days for four times. The volumes of tumors were measured with calipers at every three days for seven times and calculated according to the above equation. The tumor growth inhibition rate (TGI, %) was calculated by the formula of TGI = $(1 - V_{\text{treatment}}/V_{\text{control}}) \times 100\%$. After all treatment cycles, mice were carried out euthanasia, and tumors and major organs (heart, liver spleen, kidneys) were isolated for hematoxylin and eosin staining (H&E) and immunohistochemistry analysis (Ki-67, TUNEL).⁴¹

2.13 *Ex vivo* imaging studies

Six weeks mice bearing 4T1 xenograft tumors were intravenously injected with 100 μL of DOX, DOX@KNPs and DOX@KSA-NGs (equivalent dose: 5 mg DOX per kg body weight) or saline (as control) via the tail vein. After 24 h, mice were sacrificed and major organs and tumors were separated from the treated mice for *ex vivo* fluorescence imaging using the EX In-Vivo Imaging System (CRI Maestro, Boston, USA). The excitation and emission wavelengths were 475 and 585 nm (DOX).⁴²

3. Results and discussion

3.1 Synthesis and characterization of KNPs and KHA-NGs

KNPs and KHA-NGs were synthesized following a simple procedure in a neutral aqueous solution using keratin (40–60 kDa, Fig. S1†) and hyaluronic acid (10 kDa) as raw materials. A

digestive solvent system composed of urea, thiourea, and Tris-HCl was carefully tuned to control the degree of hydrogen bond formation between keratin and HA molecules. In the preparation process of KNPs, we observed particles precipitate characterized by nanoparticulate accumulations due to the repeat formation of disulfide bonds. The yellowish keratin solution was gradually changed to a opalescent system, and there were particles precipitated out. Fig. 1a shows the TEM micrograph of KNPs. The particle size measurement by means of DLS yielded a z -average value of 50 ± 6.4 nm and a PDI of 0.174 ± 0.021 (Fig. 1c). In the preparation process of KHA-NGs, with the removal of salts through dialysis, keratin and HA molecules were interacted with each other *via* hydrogen bonding. After the subsequent oxidation reaction, KHA-NGs were obtained containing hyaluronic acid and keratin, due to the hyaluronic acid molecules were entangled in the cross-

linking structure (Scheme 1). No precipitation was observed in the dispersion of KHA-NGs due to the good hydrophilicity endowed by hyaluronic acid, which means that KHA-NGs could be well dispersed in aqueous solution. Fig. 1b and c show the TEM micrograph, particle size and PDI of KHA-NGs (60 ± 4.1 nm, PDI 0.167 ± 0.024).

The hydroxyl and carboxyl groups on the nanogel surface endowed KNPs and KHA-NGs with a negative surface charge of -21.2 and -47.6 mV, respectively (Fig. 1d). The difference in zeta potential indicated that hyaluronic acid existed on the surface of KHA-NGs. These nanomaterials, which have negative charge on the surface, could carry positively charged drug DOX by electrostatic interaction. Particle sizes and PDI were detected using a DLS measurement (DOX@KNPs: 80 ± 5.7 nm, PDI = 0.211 ± 0.019 , DOX@KHA-NGs: 80 ± 4.2 nm, PDI = 0.217 ± 0.016 , Fig. 1c). The zeta potential of DOX@KNPs and

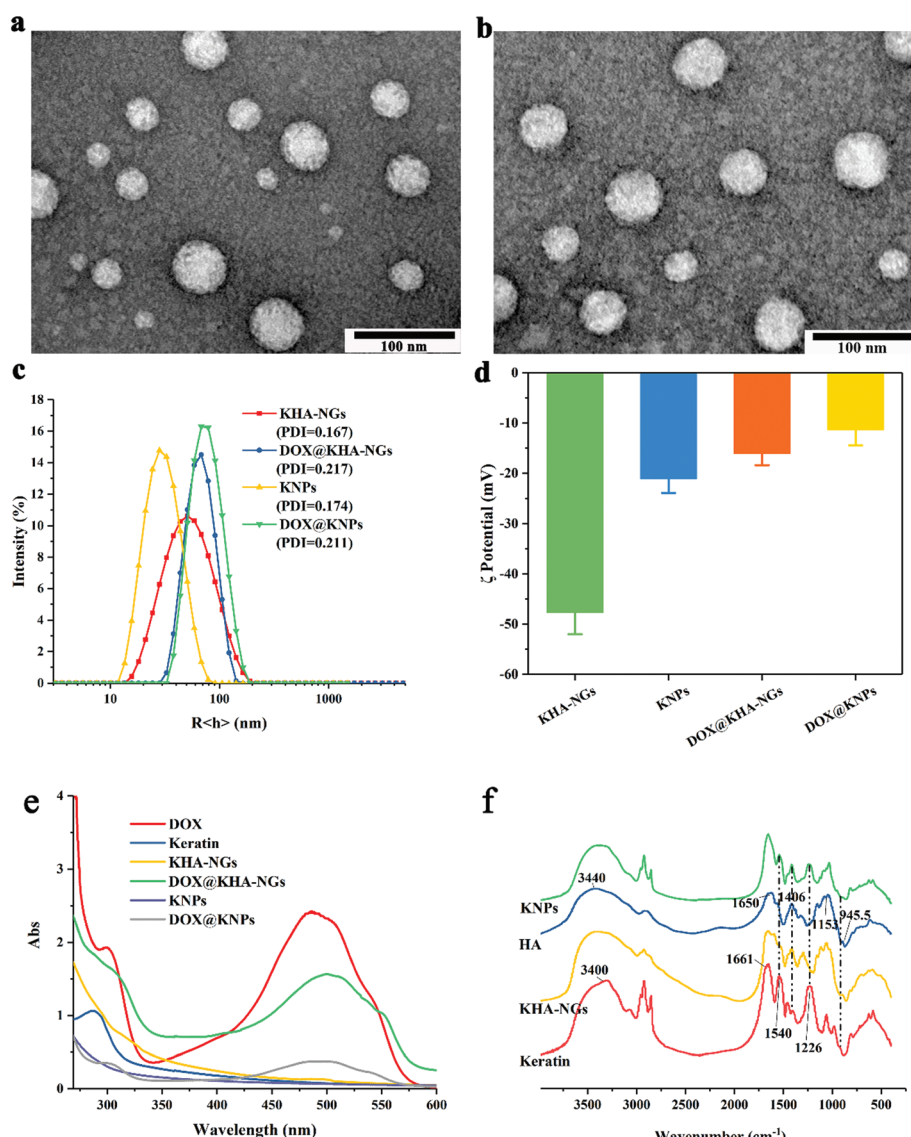


Fig. 1 Transmission electron microscopy (TEM) images of (a) KNPs and (b) KHA-NGs, the scale bars correspond to 100 nm; (c) size, PDI and (d) zeta potential of KHA-NGs, DOX@KHA-NGs, KNPs and DOX@KNPs; (e) UV-vis absorbance spectra and (f) FT-IR spectra.

DOX@KHA-NGs were -16.1 ± 2.4 mV and -12.7 ± 3.1 mV (Fig. 1d). It has been reported that negatively charged nanoparticles display a slow or reduced opsonization by the immune system.^{43,44} Thus, we hypothesized that the designed DOX@KNPs and DOX@KHA-NGs have relative low toxicity in the body, which can be used for drug delivery *in vivo*.

In the UV-vis spectra (Fig. 1e), keratin exhibited an absorption peak at 274 nm, distinct from the characteristic absorption peaks observed for KNPs and KHA-NGs, likely due to the protein structure changes. Further, a maximum absorbance of DOX at 480 nm was observed for DOX@KNPs and DOX@KHA-NGs, which confirmed that the nano-carriers successfully loaded the drug.

FT-IR spectroscopy analyses showed a broad peak approaching 3440 cm^{-1} for samples containing HA (Fig. 1f), belonging to the stretching vibrations of hydrogen bonded ($-\text{O}-\text{H}$) groups, as well as two peaks at 1406 and 1611 cm^{-1} respectively assigned to the symmetric and asymmetric stretching vibrations of $-\text{C}=\text{O}$. The peaks found in the $1250\text{--}1000\text{ cm}^{-1}$ region were assigned to the various vibrations of the carbohydrate ring.⁴⁵ The absorption peaks at 1650, 1540, and 1226 cm^{-1} observed in samples containing keratins were attributed to amide I, II, and III bands (amide I band ($\sim 1600\text{ cm}^{-1}$) – $\text{C}=\text{O}$ stretching vibrations, amide II ($\sim 1540\text{ cm}^{-1}$) – associated with N-H bending and a contribution of the $-\text{C}=\text{N}$ stretching vibrations, and amide III ($1300\text{--}1200\text{ cm}^{-1}$) due to the $-\text{N}-\text{H}$ bending and stretching vibrations from C-C and C-N), respectively. The KNP spectral data showed similar characteristics to keratin, with slight differences observed on the peaks of amide bands due to the impact of the crosslinking structure. The spectral data from the KHA-NGs sample contains the characteristics of both keratin and HA, with the presence of three main protein absorption bands (amide I-III). In addition, the peak at approximately 1100 cm^{-1} indicates the absorption of protein-associated sugar chains and thus the incorporation of glycosylated proteins in KHA-NGs.

CD spectra were used to detect the keratin conformation changes during the formation of nanogels. The spectra of keratin, keratin-HA, and KHA-NGs in aqueous solution (Fig. 2a) showed four pivotal peaks of keratin and keratin-HA mixture samples on the CD spectra, with a positive peak at approximately 194 nm and three negative peaks at approximately 207, 224, and 232 nm, indicating that the keratin chains were mainly in the α -helix conformation with a small quantity being in random coil conformation in the aqueous solution. No further perceptible bands were detected for the KHA-NGs sample, likely due to the degree of crosslinking affecting the secondary structure of keratin, leading to a change in the optical activity of nanogels. The keratin-HA mixture showed a stronger optical activity than that of pure keratin, likely due to the stretching of keratin chains upon interaction with HA chains, bringing about a more obvious secondary structure conformation in aqueous solution.⁴⁶ Secondary structure statistic of keratin and KHA solution (Fig. 2b) showed a right helix and antiparallel conformation

change in KHA solution compared to that of keratin, proving the occurrence of a hydrogen bond interaction between keratin and HA. Conversely, a decrease in optical activity was observed after crosslinking on account of coiling of the keratin molecular chain, which indicated that the formation of disulfide bonds led to changes in the keratin structure.

The chemical state of elements in KHA-NGs was detected by XPS before and after crosslinking. The XPS spectra and S 2p spectra of KHA-NGs showed a peak shift from 163.5 to 169.2 eV (Fig. 2c), attributed to the formation of K-S-S-K from K-S-H,⁴⁷ where K is the keratin protein chain linked to the β -carbon atom in cysteine. Indeed, this peak shift is an evidence of the reaction between $-\text{SH}$ groups. Cysteine disulfide K-S-S-K groups subjected to oxidative degradation may be transformed into sulfur oxides K-S(=O)-S-K, K-S(=O)₂-S-K (at 168–169 eV) and KSO₃H (at ~ 167 eV). Consequently, the increase in surface energy leads to an inter-chain interaction *via* hydrogen bonding of the sulfur oxide groups in aqueous solution.⁴⁸

The formation of nanogels occurs in two steps. Firstly, the hydroxyl, carboxyl, amino, and hydroxyl groups of the keratin and HA molecules easily interact with each other. Following dialysis, these groups form extensive hydrogen bonding, with an intertwining of keratin and HA molecules to form loose networks (KHA). Keratin is rich in thiol groups rooted in cysteine, which can form disulfide bonds through an oxidizing reaction. Following addition of the H₂O₂ solution, the $-\text{SH}$ group in keratin oxidizes to form disulfide bonds, leading to keratin chain self-assembly and finally to the formation of KHA-NGs.

3.2 Stimuli-response and controlled release profile

Drug loading capacity, stability, and release behavior are important parameters for drug carriers. Drug carriers should successfully load pharmaceutical molecules as well as stabilize these in the hematologic microenvironment, subsequently releasing them into targeted tissues under physiological stimulation.^{49–51} The DOX loading capacity of KHA-NGs was quantified by UV-vis spectrophotometry on the basis of a standard curve (Fig. S3†). The loading efficiency and embedding ratio of KNPs and KHA-NGs were approximately 18.9% and 81.2% *vs.* 54.1% and 77.4%, respectively. The difference in values is likely attributable to the characteristics of keratin and hyaluronan. Coulombic force is the main force of KHA-NGs and DOX molecules.⁵² Both keratin and hyaluronan chains are negatively charged molecules able to undergo electrostatic interactions with positively charged DOX molecules.³⁶ The zeta potential of KNPs, KHA-NGs, DOX@KNPs, and DOX@KHA-NGs were -21.2 , -47.6 , -12.1 , and -16.9 eV, respectively (Fig. 1d), which testified the interaction between them *via* electrostatic force. Thus, the considerable extent of DOX bonding to KHA-NGs led to an obvious decrease in zeta potential. Further, both keratin and hyaluronan are natural macromolecules with abundant side groups on their molecule chain. Hydrogen bonding interactions between these side groups and DOX molecules increased the capacity of nanogels

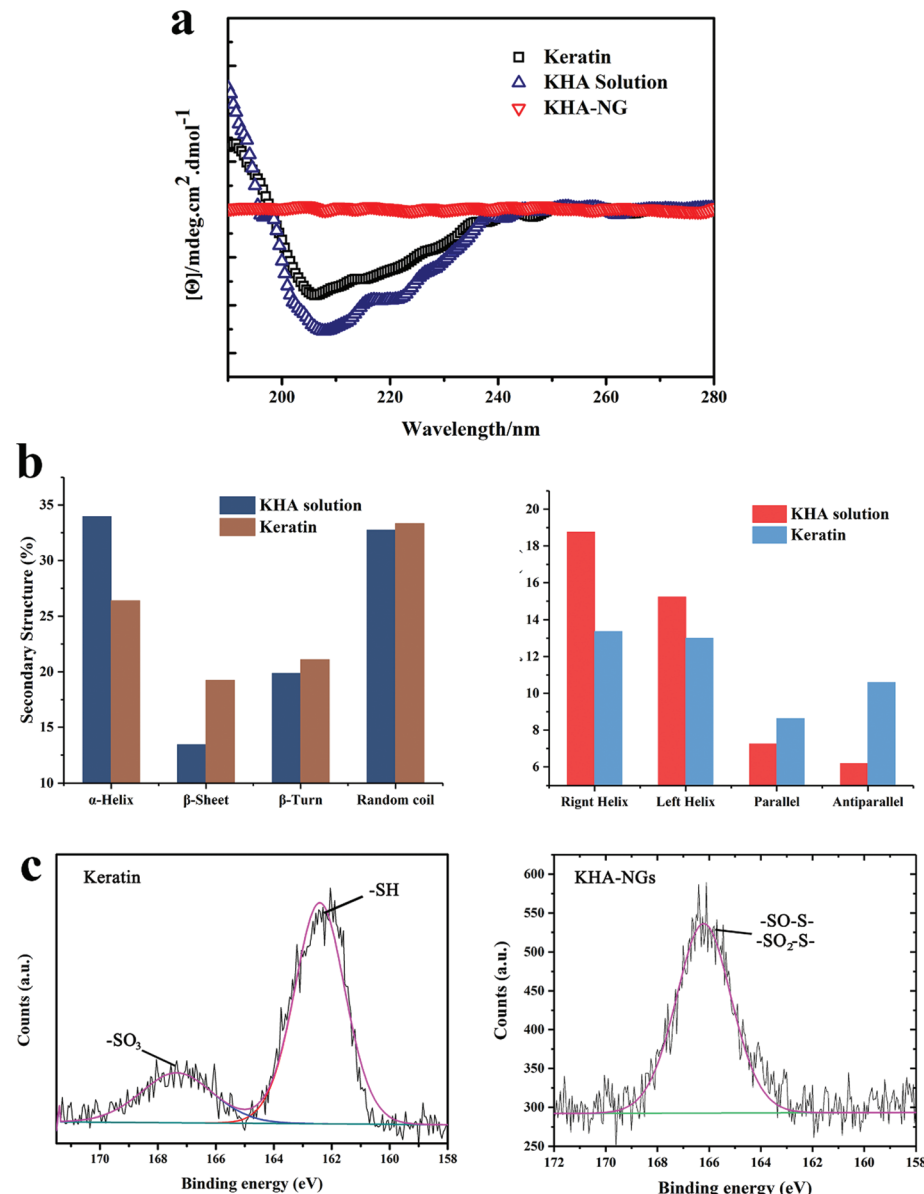


Fig. 2 (a) Circular dichroism spectrum (CD) of keratin, KHA solution and KHA-NGs; (b) secondary structure statistic of keratin and KHA solution; (c) XPS spectra of the S 2p peak of keratin and KHA-NGs.

to encapsulate the drug. Thus, the higher DOX loading capacity of KHA-NGs is attributed to its low zeta potential.

We next investigated the stimuli-response and *in vitro* DOX release of DOX@KNPs and DOX@KHA-NGs in various bio-mimetic solutions. As shown in Fig. 3a and b, the release of DOX increased under acidic condition with high GSH concentration and trypsin. To be specific, in pH 7.4 PBS solution as control group, which corresponded to the blood pH level, only 14% of DOX was delivered after 48 min from DOX@KNPs and 12% from DOX@KHA-NGs. Regarding the release at pH 5.5, the release of DOX was accelerated and total release amount were about 40% due to the protonation. As buffer acidity increased, the negatively charged carboxylates (COO^-) of KNPs and KHA-NGs got the protons and were neu-

tralized. The protonation weakened the electrostatic interaction between DOX and nano-carriers and therefore facilitated DOX diffusion leading to the accelerated release. The GSH concentrations used herein (10 μM and 10 mM) are similar to those found in blood plasma and in tumour cells, respectively. Only 15% of DOX was released from DOX@KHA-NGs and 19% from DOX@KNPs after 45 min in 10 μM GSH in pH 7.4 solution. Approximately 30% of DOX was released from DOX@KHA-NGs and 40% from DOX@KNPs after 45 min with 10 mM GSH in pH 7.4 solution due to nanogel swelling by disulfide bond cracking. This suggested that high concentrations of GSH could promote drug release. Approximately 81% of DOX was released from DOX@KHA-NGs and 84% from DOX@KNPs in the presence

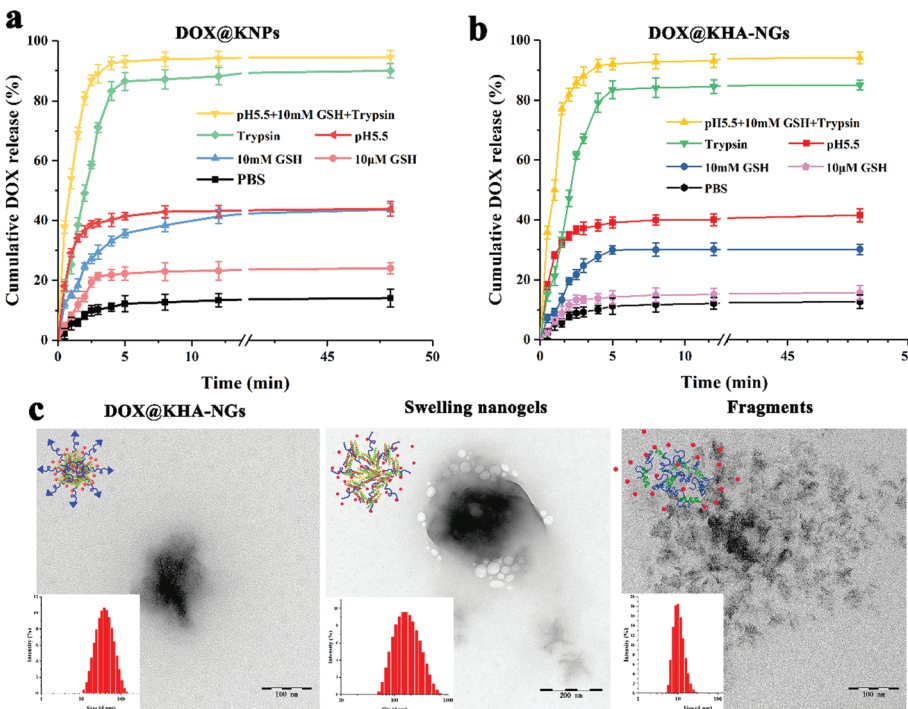


Fig. 3 DOX release profiles of (a) DOX@KNPs and (b) DOX@KHA-NGs in different biomimetic solutions at 37 °C (pure pH 7.4 PBS solution, pH 7.4 PBS solution with 10 μM GSH, with 10 mM GSH, with trypsin, pure pH 5.5 PBS solution, pH 5.5 PBS solution with 10 mM GSH + 0.04 mM trypsin); (c) high resolution transmission electron microscopy (HRTEM) images of stimuli response process of DOX@KHA-NGs.

of trypsin alone, which indicated that the nanogels had enzymatic stimuli-response. The release amount and release ratio of DOX@KNPs were higher than those of DOX@KHA-NGs, because the keratin was more exposed to enzyme and GSH interactions without the presence of HA. Additionally, in the presence of 10 mM GSH and trypsin in pH 5.5 condition, the nanogels could release the drug rapidly in large quantities. More than 75% of the encapsulated DOX was released from DOX@KHA-NGs and DOX@KNPs within the first 3 min, and more than 90% of the loaded DOX was released after 8 min in the presence of trypsin and 10 mM GSH at pH 5.5. The coexistence of trypsin and high concentration GSH at lower pH value would lead to a rapid DOX release based on the synergistic effect of protonation and nano-carrier disassembly due to the keratin backbone degradation. It is reported that the extracellular pH values of most malignant tumor tissues are lower (pH 6.0–7.0) than that of the normal tissues and blood (pH 7.4), and even decreasing further in lysosomes and endosomes (5.5–6.0).⁵³ Besides, the concentrations of GSH in lysosomes and endosomes (>10 mM) are much higher than that in the bloodstream and extracellular of normal tissue (~10 μM).^{42,54} Thus, the release of DOX would be facilitated under the acidic environment and high concentration GSH in tumor tissue or inside the tumor cells. Enzymes in lysosomes would further promote the drug release due to the degradation of nano-carriers. This bio-responsive property of KHA-NGs may steadily retain the drug in the biomimetic

physiological condition and generate sufficient DOX release within lysosomes and endosomes.

The morphology of nanogels was observed by high-resolution TEM after treatment with the various conditions. A stable swelling-cracking of the nanogels occurred during the release process in all conditions (Fig. 3c). Thus, this stimuli-responsive drug delivery system could adapt to the hematophysiologic environment and release drugs within tumor-specific sites.^{55,56} The prepared nanogels are stable in a physiological environment due to the entanglement of keratin and hyaluronan chains after crosslinking. Yet, at high GSH concentrations, the disulfide bonds in the thiol groups, which led to nanogel swelling, can be ruptured. Moreover, keratin can be digested into polypeptides by trypsin, leading to the deconstruction of the nanogels to smaller particles or even fragments. Thus, as is depicted in Scheme 1, the DOX molecules are embedded within the crosslinked KHA-NGs through electrostatic force and hydrogen bonding. DOX@KHA-NGs are stable in the physiological environment due to the hydrophilic property of hyaluronan molecules. Indeed, the nanogels underwent the swelling-cracking process and DOX release only when the nanogels were taken up by the tumor cells. This was attributed to the higher intracellular GSH and trypsin concentrations in tumor cells than under blood homeostasis.^{42,54} Consequently, KHA-NGs have a dual-stimuli responsive property which can prevent premature leakage of antitumor drugs and delivery of drugs within tumor-specific conditions.

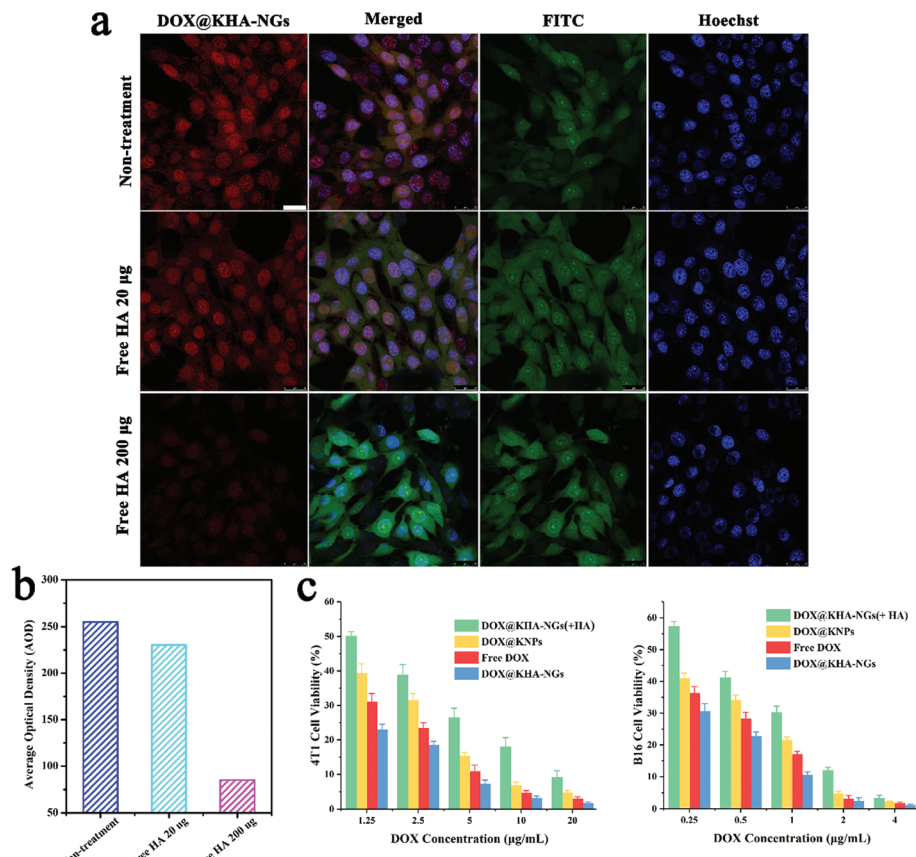


Fig. 4 (a) Cellular uptake of DOX@KHA-NGs (DOX concentration = 5 $\mu\text{g mL}^{-1}$) by 4T1 cells with free HA (20 and 200 $\mu\text{g mL}^{-1}$) or without free HA after 4 h incubation (scale bar = 25 μm). (b) Average optical density (AOD) statistics. (c) Cell viabilities of 4T1 cell lines and B16 cell lines after being incubated with DOX, DOX@KNPs, DOX@KHA-NGs and DOX@KHA-NGs pretreated with free HA (200 $\mu\text{g mL}^{-1}$) at different dosages for 48 h.

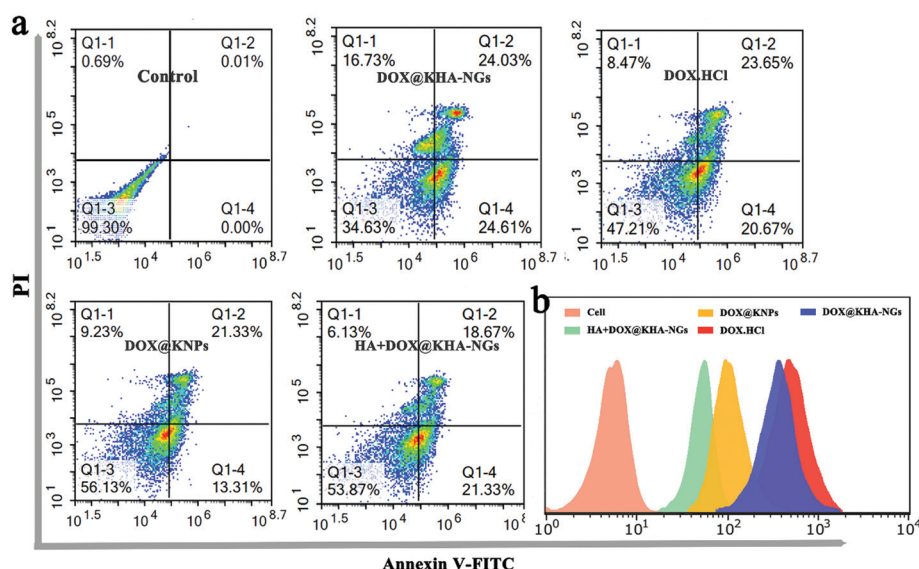


Fig. 5 (a) Apoptosis results of 4T1 cells incubated with DOX, DOX@KNPs, DOX@KHA-NGs and DOX@KHA-NGs + HA for 24 h. (b) Flow cytometry quantitative analyses of various drug formulations after incubation with 4T1 cells for 4 h (DOX-equivalent dose: 5 $\mu\text{g mL}^{-1}$).

3.3 CD44-targeting DOX delivery and *in vitro* antitumor activity

The CD44-targeting DOX delivery antitumor effect of DOX@KHA-NGs was evaluated in the 4T1 cell line, which expresses high levels of CD44 receptors. A strong fluorescence of DOX was detected in the nuclei of 4T1 cells following 4 h incubation with DOX@KHA-NGs (CLSM and average optical density statistics results), while the fluorescence was negligible in the cells pretreated with 200 $\mu\text{g mL}^{-1}$ free HA (Fig. 4a and b), indicating an efficient uptake of DOX@KHA-NGs by 4T1 cells and fast intracellular drug release. The remarkable cellular uptake of DOX@KHA-NGs was due to the presence of HA in the nanogels, which bound specifically to the CD44 receptors of 4T1 cells; internalization was obviously inhibited by the addition of free HA.

The cytotoxicity of DOX, DOX@KNPs, and DOX@KHA-NGs on the proliferation of CD44-positive cells (4T1 and B16 cells)

and CD44-negative cells (4T1 and B16 cells pretreated with 200 $\mu\text{g mL}^{-1}$ free HA) was further quantitatively assessed by the CCK-8 assay. For this purpose, DOX, DOX@KNPs, and DOX@KHA-NGs were cultured at specific concentrations with 4T1 (1.25, 2.5, 5, 10, and 20 $\mu\text{g mL}^{-1}$) and B16 (0.25, 0.5, 1, 2, and 4 $\mu\text{g mL}^{-1}$) for 48 h. DOX, DOX@KNPs, and DOX@KHA-NGs displayed a dose-dependent cytotoxicity in all cell lines (Fig. 4c). After 48 h of incubation, for both 4T1 and B16 cells, DOX@KNPs showed a lower inhibition effect than free DOX due to the increased likelihood of DOX molecules being taken. Notably, DOX@KHA-NGs showed a better inhibition effect than DOX to cancer cells in a dose-dependent manner. However, the antitumor activity of DOX@KHA-NGs was significantly reduced by the pretreatment of cells with free HA. These results indicate that DOX@KHA-NGs possess an apparent targetability to CD44-positive cells and can efficiently deliver and release DOX within the target cancer cells, inducing a high antitumor efficacy. Normal cells, such as mouse

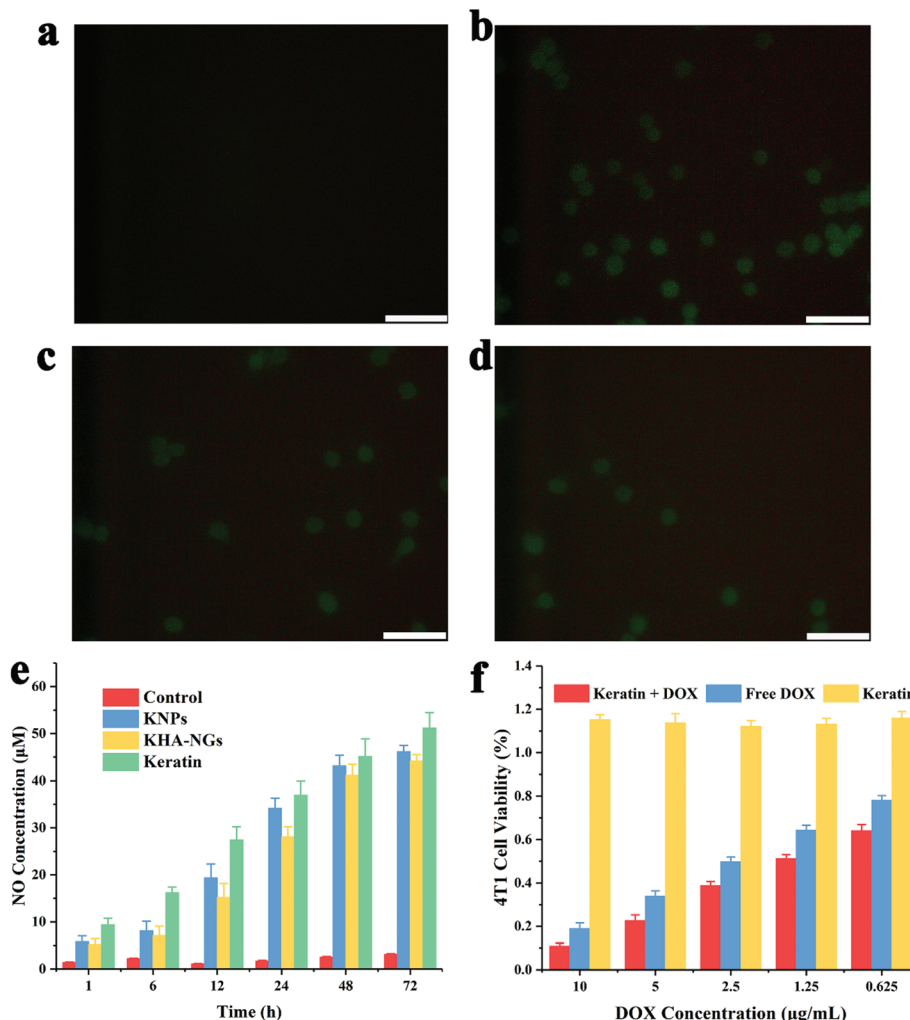


Fig. 6 Intracellular NO release of 4T1 cells treated with (a) colorless medium, (b) 25 μg keratin, (c) KNPs and (d) KHA-NGs. NO was stained with a fluorescent indicator (3-amino,4-aminomethyl-2',7'-difluorescein, diacetate, scale bar = 100 μm). (e) NO release as the function of time. (f) Viability of 4T1 cells after being incubated with keratin, DOX and keratin + DOX at different concentration for 48 h.

fibroblast cells (L929) and mouse embryonic fibroblast cells (NIH-3T3), were used to detect the cytotoxicity of KHA-NGs, showing that there was no obvious cytotoxicity at any given concentration against these two cell lines (Fig. S3†).

The apoptosis results of 4T1 cells induced by various drug formulations were shown in Fig. 5a. DOX@KHA-NGs and DOX resulted in a late apoptotic ratio of 24.03% and 23.65%, respectively, in 4T1 cells, yet pretreatment with free HA induced a lower apoptosis of 4T1 tumor cells of 18.67%.

DOX@KNPs led to a late apoptotic ratio of 21.33%. The above results imply that DOX@KHA-NGs can effectively internalize into CD44-positive cells and induce apoptosis.

The intracellular uptake of 4T1 against different drug formulations were detected using flow cytometry quantitative analyses (Fig. 5b). The results showed that a slightly higher level of uptake was obtained in DOX than DOX@KHA-NGs, due to the diffusion of DOX as an amphiphilic small molecule. The DOX@KNPs and DOX@KHA-NGs pretreated with 200 $\mu\text{g mL}^{-1}$

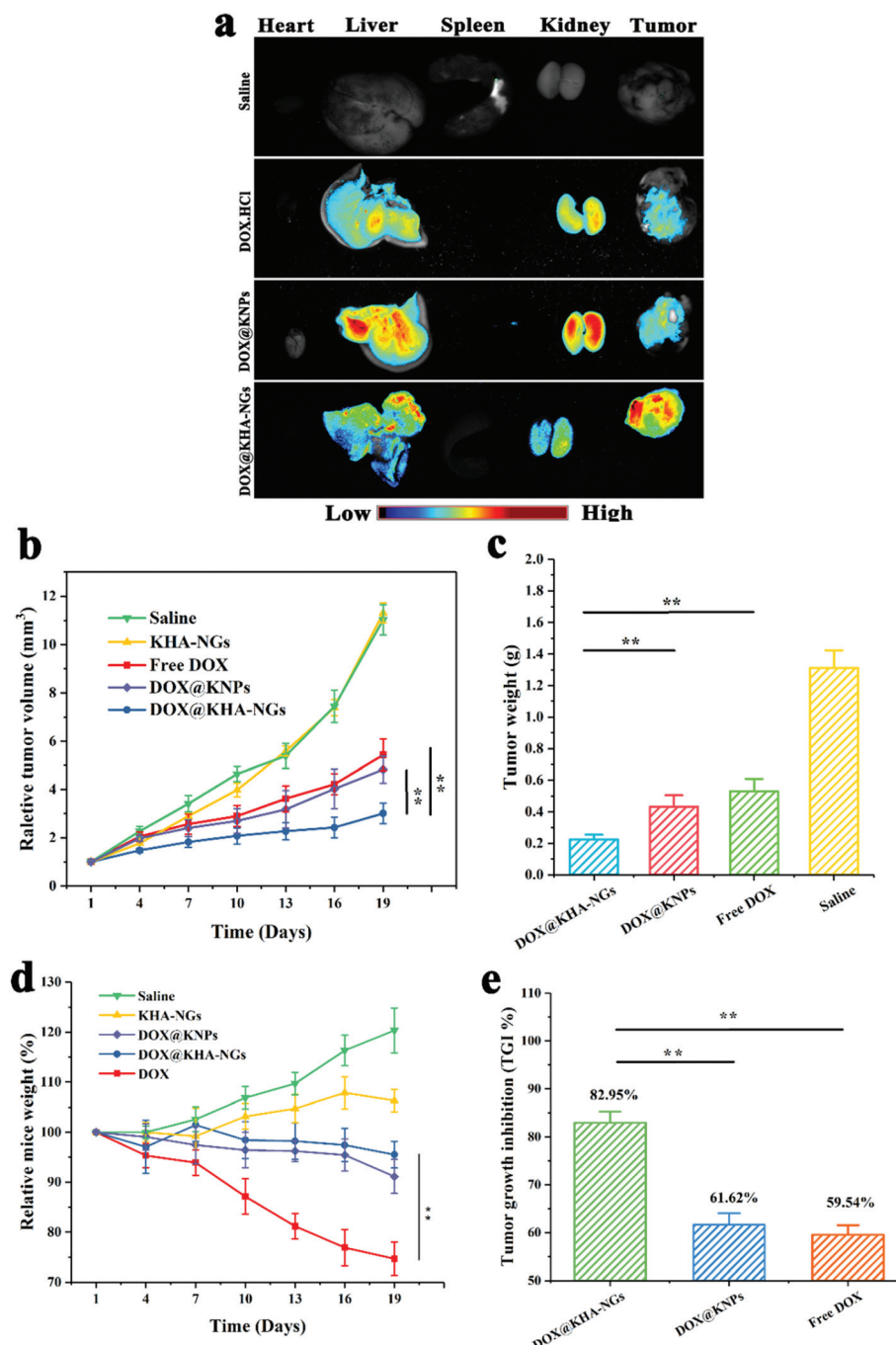


Fig. 7 (a) Drug distribution of DOX, DOX@KNPs and DOX@KHA-NGs in major organs and tumors after intravenous injection for 24 h. (b) Relative tumor volume. (c) Tumor weight of each group. (d) Relative mice weight and (e) TGI. (Means \pm standard deviation, $n = 5$, $**P < 0.01$.)

of HA showed a lower level of uptake due to the occupied receptor sites. These results are in agreement with those of CLSM (Fig. 4a).

3.4 NO release and enhanced anticancer activity *in vitro*

NO, an endogenously synthesized small molecule, had a potential in cancer therapy due to its synergistic antitumor capability.²⁵ In this study, we examined that keratin promoted the production of NO in 4T1 cells. Both intracellular NO levels and the potential of catalyzing NO release were tested. Fluorescence images (Fig. 6a and b) showed that the intracellular NO production was significantly increased by keratin. KNPs and KHA-NGs could also promote the intracellular NO production (Fig. 6c and d). These results suggested that, in the presence of keratin, cells could produce NO to a certain extent.

GSNO is a kind of endogenous donors, which could release NO under certain conditions.²³ We then detected the release of NO from GSNO in the presence of keratin, KNPs and KHA-NGs. The results of NO release as a function of time showed that the amounts of NO release in the presence of keratin, KNPs and KHA-NGs were significantly higher than that of control group (Fig. 6e). Therefore, keratin could induce cell to produce NO by promoting the release of NO from GSNO. After that, we studied the synergistic anticancer efficacy

of keratin. Fig. 6f showed that the viability values of 4T1 cells cultured with keratin alone were 1.0–1.1, which indicated that keratin had no cytotoxicity against 4T1 cells. However, the viabilities of keratin and DOX combination group were lower than that of DOX alone. This demonstrated that keratin achieved synergistic anticancer effect by promoting the production of NO in tumor cells.

3.5 *In vivo* anticancer activities of DOX@KHA-NGs

Motivated by the satisfactory performances of *in vitro* cytotoxicity and target activity of DOX@KHA-NGs, we further evaluated targeted and therapeutic efficacy *in vivo*. *Ex vivo* fluorescence imaging was used to analyze the distribution of drugs in tumors and main organs (Fig. 7a). Semi-quantitative fluorescence intensity statistics were shown in Fig. S5.[†] Clearly, both DOX@KNPs and DOX@KHA-NGs had stronger fluorescence signals at the solid tumor site than the DOX-treated group due to the EPR effect and active target effect. Additionally, the fluorescence signal of DOX@KHA-NGs group at tumor site was stronger than that of DOX-treated. This observation was ascribed to CD44 active targeting and EPR effects. Minimal drug signals were captured in other organs such as the liver and kidney in the DOX@KHA-NGs group,

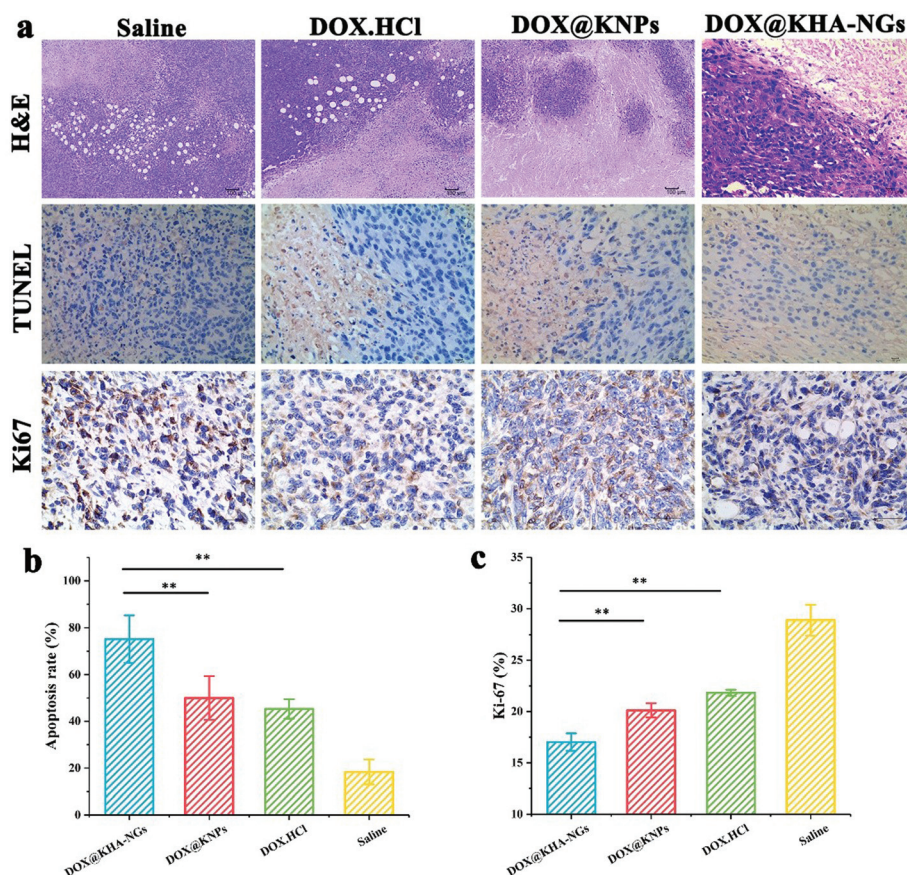


Fig. 8 (a) Histological and immunohistochemical analysis of H&E, TUNEL and Ki-67 assays for 4T1 tumors. TUNEL-positive cells and Ki-67-positive cells are stained brown. (b) Apoptotic index. (c) The mean density of Ki-67. (Means \pm standard deviation, $n = 5$, ** $P < 0.01$)

whereas the DOX-treated group showed a much stronger signal.

Rapid tumor growth was observed in saline- and KHA-NG-treated mice (Fig. 7b) due to their non-cytotoxicity and the lack of an anti-tumor effect both *in vitro* and *in vivo*. Additionally, the average tumor weight in treated mice was lower than that in the control groups. Compared to other groups, the DOX@KHA-NGs group exhibited maximal antitumor activity, with an average tumor weight less than half of the DOX groups' (Fig. 7c). Additionally, the body weight of tumor-bearing mice in the DOX@KHA-NGs group showed no apparent decrease compared to the DOX-treated group (Fig. 7d). The TGI rates of DOX@KHA-NGs reached approximately 83% (Fig. 7e), showing a much enhancive efficacy compared to DOX@KNPs- and DOX-treated groups (62% and 59%, respectively, ** $p < 0.01$).

Histological and immunohistochemical analyses were used to further evaluate the antitumor activity. In relation to the other three groups, most areas of the tumor were observed to be necrotic, the contours of the cells were not clear and the tumor tissue could see the fragments of the protein-like substance in DOX@KHA-NGs group (Fig. 8a). The immunohistochemical results also illustrated that DOX@KHA-NGs could eliminate Ki-67 positive proliferative tumor cells and induced apoptosis of tumor cell (TUNEL-positive). At the end of the treatment course, the major organs of mice in all treatment groups were collected for H&E staining. The organs showed no significant damage, in contrast with the control groups, suggesting that DOX@KHA-NGs had no apparent side effects (Fig. S4†). Combined with histological analysis (Fig. 8b), DOX@KHA-NGs exhibited a more effective antitumor activity than free DOX and DOX@KNPs, with negligible systemic toxicity.

4. Conclusions

Herein, we prepared CD44-targeted nanogels with tumor microenvironment responsiveness based on HA and human hair keratin. These nanogels had nanostructures and negatively charged surface which were able to embed large amount of anticancer drugs (DOX) and transported them to the tumor site. Moreover, receptor-mediated active targeting (CD44 receptor) increased the drug accumulation at the tumor sites and cell internalization. Further, KHA-NGs were able to improve intracellular NO levels and enhance the anticancer efficacy of chemotherapy drugs. *In vitro* and *in vivo* results verified that these functional nanogels could suppress tumor growth with milder side effects compared to free DOX. These results were obtained through the successful utilization of the structural/functional features of keratin and HA to achieve a highly tumor-specific treatment.

Conflicts of interest

There are no conflicts to declare.

Acknowledgements

This work is supported by the National Key Program for Research and Development of China (No. 2016YFC1102700), the National Basic Research Program of China (No. 2012CB933600), National Natural Science Foundation of China (No. 51373106) and Sichuan Science and Technology Program Key Projects (No. 2017JY0018). The authors thank Yutong He, Yangmei Chen and Boyao Wu for providing hair.

References

- 1 R. Xu, G. Zhang, J. Mai, X. Deng, V. Segura-Ibarra, S. Wu, J. Shen, H. Liu, Z. Hu, L. Chen, Y. Huang, E. Koay, Y. Huang, J. Liu, J. E. Ensor, E. Blanco, X. Liu, M. Ferrari and H. Shen, *Nat. Biotechnol.*, 2016, **34**, 414–418.
- 2 Z. Chen, C. Wang, J. Chen and X. Li, *J. Am. Chem. Soc.*, 2013, **135**, 4179–4182.
- 3 S. E. Kim, L. Zhang, K. Ma, M. Riegman, F. Chen, I. Ingold, M. Conrad, M. Z. Turker, M. Gao, X. Jiang, S. Monette, M. Pauliah, M. Gonen, P. Zanzonico, T. Quinn, U. Wiesner, M. S. Bradbury and M. Overholtzer, *Nat. Nanotechnol.*, 2016, **11**, 977–985.
- 4 W. Wei, X. Zhang, X. Chen, M. Zhou, R. Xu and X. Zhang, *Nanoscale*, 2016, **8**, 8118–8125.
- 5 Q. Wang, M. Shen, T. Zhao, Y. Xu, J. Lin, Y. Duan and H. Gu, *Sci. Rep.*, 2015, **5**, 7774.
- 6 P. Laskar, B. Saha, S. K. Ghosh and J. Dey, *RSC Adv.*, 2015, **5**, 16265–16276.
- 7 M. Alhijjaj, J. Bouman, N. Wellner, P. Belton and S. Qi, *Mol. Pharm.*, 2015, **12**, 4349–4362.
- 8 S. Sunoqrot, J. Bugno, D. Lantvit, J. E. Burdette and S. Hong, *J. Controlled Release*, 2014, **191**, 115–122.
- 9 H. Zhang, Z. Yi, Z. Sun, X. Ma and X. Li, *J. Mater. Chem. B*, 2017, **5**, 7622–7631.
- 10 F. Dosio, S. Arpicco, B. Stella and E. Fattal, *Adv. Drug Delivery Rev.*, 2016, **97**, 204–236.
- 11 G. Tripodo, A. Trapani, M. L. Torre, G. Giannonna, G. Trapani and D. Mandracchia, *Eur. J. Pharm. Biopharm.*, 2015, **97**, 400–416.
- 12 S. Y. Qin, A. Q. Zhang, S. X. Cheng, L. Rong and X. Z. Zhang, *Biomaterials*, 2017, **112**, 234–247.
- 13 B. Pelaz, *et al.*, *ACS Nano*, 2017, **11**, 2313–2381.
- 14 X. Yang, X. Zhang, Z. Liu, Y. Ma, Y. Huang and Y. Chen, *J. Phys. Chem. C*, 2008, **112**, 17554–17558.
- 15 K. Cai, X. He, Z. Song, Q. Yin, Y. Zhang, F. M. Uckun, C. Jiang and J. Cheng, *J. Am. Chem. Soc.*, 2015, **137**, 3458–3461.
- 16 S. Xu, L. Sang, Y. Zhang, X. Wang and X. Li, *Mater. Sci. Eng., C*, 2013, **33**, 648–655.
- 17 Z. Sun, Z. Yi, H. Zhang, X. Ma, W. Su, X. Sun and X. Li, *Carbohydr. Polym.*, 2017, **175**, 159–169.
- 18 Z. Yi, Z. Sun, G. Chen, H. Zhang, X. Ma, W. Su, X. Cui and X. Li, *J. Mater. Chem. B*, 2018, **6**, 1373–1386.

- 19 A. Hervault, A. E. Dunn, M. Lim, C. Boyer, D. Mott, S. Maenosono and N. T. Thanh, *Nanoscale*, 2016, **8**, 12152–12161.
- 20 Y. Tian, X. Jiang, X. Chen, Z. Shao and W. Yang, *Adv. Mater.*, 2014, **26**, 7393–7398.
- 21 M. Curcio, B. Blanco-Fernandez, L. Diaz-Gomez, A. Concheiro and C. Alvarez-Lorenzo, *Bioconjugate Chem.*, 2015, **26**, 1900–1907.
- 22 H. O. Haddar, T. I. Zaghloul and H. M. Saeed, *Biodegradation*, 2009, **20**, 687–694.
- 23 X. Jin, Y. Wang, J. Yuan and J. Shen, *Mater. Lett.*, 2016, **175**, 188–190.
- 24 Y. Li, X. Zhi, J. Lin, X. You and J. Yuan, *Mater. Sci. Eng., C*, 2017, **73**, 189–197.
- 25 A. B. Seabra, G. Z. Justo and P. S. Haddad, *Biotechnol. Adv.*, 2015, **33**, 1370–1379.
- 26 F. Danhier, *J. Controlled Release*, 2016, **244**, 108–121.
- 27 H. Maeda, *Cancer Sci.*, 2013, **104**, 779–789.
- 28 C. Lee, H. S. Hwang, S. Lee, B. Kim, J. O. Kim, K. T. Oh, E. S. Lee, H. G. Choi and Y. S. Youn, *Adv. Mater.*, 2017, **29**(13), 1605563.
- 29 F. Ravar, E. Saadat, M. Gholami, P. Dehghankelishadi, M. Mahdavi, S. Azami and F. A. Dorkoosh, *J. Controlled Release*, 2016, **229**, 10–22.
- 30 X. Guo, L. Wang, K. Duval, J. Fan, S. Zhou and Z. Chen, *Adv. Mater.*, 2018, **30**(3), 1705436.
- 31 Y. Wang, G. Wei, X. Zhang, F. Xu, X. Xiong and S. Zhou, *Adv. Mater.*, 2017, **29**(12), 1605357.
- 32 C. Shi, X. Guo, Q. Qu, Z. Tang, Y. Wang and S. Zhou, *Biomaterials*, 2014, **35**, 8711–8722.
- 33 X. Guo, L. Wang, X. Wei and S. Zhou, *J. Polym. Sci., Part A: Polym. Chem.*, 2016, **54**, 3525–3550.
- 34 T. F. Martens, K. Peynshaert, T. L. Nascimento, E. Fattal, M. Karlstetter, T. Langmann, S. Picaud, J. Demeester, S. C. De Smedt, K. Remaut and K. Braeckmans, *Eur. J. Pharm. Sci.*, 2017, **103**, 27–35.
- 35 Y. Zhong, K. Goltzsche, L. Cheng, F. Xie, F. Meng, C. Deng, Z. Zhong and R. Haag, *Biomaterials*, 2016, **84**, 250–261.
- 36 Y. Zhong, J. Zhang, R. Cheng, C. Deng, F. Meng, F. Xie and Z. Zhong, *J. Controlled Release*, 2015, **205**, 144–154.
- 37 J. H. Park, H. J. Cho, H. Y. Yoon, I. S. Yoon, S. H. Ko, J. S. Shim, J. H. Cho, J. H. Park, K. Kim, I. C. Kwon and D. D. Kim, *J. Controlled Release*, 2014, **174**, 98–108.
- 38 R. Cheng, F. Meng, C. Deng and Z. Zhong, *Nano Today*, 2015, **10**, 656–670.
- 39 C. Yang, X. Wang, X. Yao, Y. Zhang, W. Wu and X. Jiang, *J. Controlled Release*, 2015, **205**, 206–217.
- 40 X. Yao, X. Niu, K. Ma, P. Huang, J. Grothe, S. Kaskel and Y. Zhu, *Small*, 2017, **13**(2), 1602225.
- 41 S. McRae Page, E. Henchey, X. Chen, S. Schneider and T. Emrick, *Mol. Pharm.*, 2014, **11**, 1715–1720.
- 42 X. Wei, Y. Wang, X. Xiong, X. Guo, L. Zhang, X. Zhang and S. Zhou, *Adv. Funct. Mater.*, 2016, **26**, 8266–8280.
- 43 H. Cabral, Y. Matsumoto, K. Mizuno, Q. Chen, M. Murakami, M. Kimura, Y. Terada, M. R. Kano, K. Miyazono, M. Uesaka, N. Nishiyama and K. Kataoka, *Nat. Nanotechnol.*, 2011, **6**, 815–823.
- 44 G. Shen, R. Xing, N. Zhang, C. Chen, G. Ma and X. Yan, *ACS Nano*, 2016, **10**, 5720–5729.
- 45 S. K. Tam, J. Dusseault, S. Polizu, M. Menard, J. P. Halle and L. Yahia, *Biomaterials*, 2005, **26**, 6950–6961.
- 46 J. Guo, S. Pan, X. Yin, Y. F. He, T. Li and R. M. Wang, *J. Appl. Polym. Sci.*, 2015, **132**(9), 41572.
- 47 M.-C. Bourg, A. Badia and R. B. Lennox, *J. Phys. Chem. B*, 2000, **104**, 6562–6567.
- 48 M. Mori and N. Inagaki, *Res. J. Text. Apparel*, 2006, **10**, 33–45.
- 49 S. Hirjarvi, C. Passirani and J.-P. Benoit, *Curr. Drug Discovery Technol.*, 2011, **8**, 188–196.
- 50 R. Mo, Q. Sun, J. Xue, N. Li, W. Li, C. Zhang and Q. Ping, *Adv. Mater.*, 2012, **24**, 3659–3665.
- 51 V. Stepanic, A. Gasparovic, K. Troselj, D. Amic and N. Zarkovic, *Curr. Top. Med. Chem.*, 2015, **15**, 496–509.
- 52 Q. Li, S. Yang, L. Zhu, H. Kang, X. Qu, R. Liu and Y. Huang, *Polym. Chem.*, 2015, **6**, 2869–2878.
- 53 D. Schmaljohann, *Adv. Drug Delivery Rev.*, 2007, **58**, 1655–1670.
- 54 W. Li, L. Huang, X. Ying, Y. Jian, Y. Hong, F. Hu and Y. Du, *Angew. Chem., Int. Ed.*, 2015, **54**, 3126–3131.
- 55 J. Kamada, K. Koynov, C. Corten, A. Juhari, J. A. Yoon, M. W. Urban, A. C. Balazs and K. Matyjaszewski, *Macromolecules*, 2010, **43**, 4133–4139.
- 56 M. Huo, J. Yuan, L. Tao and Y. Wei, *Polym. Chem.*, 2014, **5**, 1519–1528.